Available online at www.sciencedirect.com
ScienceDirect
Journal of Power Sources 171 (2007) 644–651
JOURNAL OF POWER SOURCES
www.elsevier.com/locate/jpowsour

Visualization study on the dynamics of CO_2 bubbles in anode channels and performance of a DMFC

Qiang Liao *, Xun Zhu, Xueyan Zheng, Yudong Ding

Institute of Engineering Thermophysics, Chongqing University, Chongqing 400044, China

Received 31 May 2007; received in revised form 21 June 2007; accepted 22 June 2007
Available online 12 July 2007

Abstract

The present study reports on experimental investigations of the dynamic behavior of CO_2 gas bubbles and the performance of a 9 cm^2 transparent direct methanol fuel cell (DMFC). The movement of CO_2 gas bubbles in the anode channel subjected to a flow of aqueous methanol solution was visualized. A series of parametric studies was carried out to evaluate the effects on the CO_2 gas bubbles dynamics as well as the cell performance. It was observed that the pores around the corner of the channel ribs and the intersection of the carbon cloth fibres were favorable sites for the emergence of CO_2 gas bubbles. The growth and coalescence of CO_2 gas bubbles resulted in gas slugs blocking the channel and the pores in porous diffusion layer as well. Then the gas slugs were pushed by the aqueous methanol solution flow to detach and sweep downstream, clearing all the existing small bubbles on the porous diffusion layer surface. The processes of emergence, growth, coalescence, detachment, and sweeping of the gas bubbles were found to occur periodically. High flow rates of the aqueous methanol solution resulted in small discrete CO_2 gas bubbles and short gas slugs. Increasing temperature of the methanol solution increased the quantity of CO_2 gas bubbles. More CO_2 gas bubbles and large gas slugs appeared in the channels with increasing pressure difference between the anode and the cathode. The cell performance was improved with increasing aqueous methanol flow rates, feed temperature, feed concentration, and the pressure difference between the anode and the cathode.

Keywords: Direct methanol fuel cell; CO_2 gas bubbles dynamic behavior; Visualization study; Anode channel; Cell performance

1. Introduction

Conventional batteries are becoming inadequate for the increasing power and complexity of portable electronic devices such as cell phones, laptop computers, and video recorders. Trends in portable electronics and wireless technology advances are creating a critical need for smaller, less-costly, environmentally safe, highly efficient and long-lasting power in portable energy applications. Direct methanol fuel cell (DMFC) technology with the advantages of high energy density, rapid start up and response, low operating temperature, zero emission, and refueling instantly inevitably stands out as the most promising candidate to applications of present and the next generation of portable electronic equipment [1,2]. Furthermore, DMFC has less issue over proton exchange membrane fuel cell (PEMFC) in term of fuel infrastructure because methanol is easier to be refueled, safer to be stored and simpler to be handled than hydrogen. For these reasons, DMFC research is receiving much attention in the fuel cell community in recent years [3–20].

A typical DMFC consists essentially of a membrane-electrode assembly (MEA) sandwiched between two bipolar plates which have channels for distributing the fuel (an aqueous methanol solution) and oxidant (oxygen from air). The electrodes are typically made of a random matrix of carbon fibres (carbon cloth or carbon paper), commonly referred as a porous diffusion layer. In an operating DMFC, methanol solution diffuses through one of the porous diffusion layers and is oxidized at the anode to produce carbon dioxide, protons, and electrons. At the cathode, oxygen diffuses through another porous diffusion layer and is reduced with protons passing through the proton exchange membrane as well as electrons flowing through the load from the anode to produce water. To ensure continuity and stabilization of the electrochemical reaction in an operating DMFC, CO_2 gas and water must be removed rapidly and efficiently to allow fresh fuel and oxygen to arrive at the catalyst layers. At the anode, stagnant CO_2 gas adhering to the surface

* Corresponding author. Tel.: +86 23 65102474; fax: +86 23 65102474.
E-mail address: lqzx@cqu.edu.cn (Q. Liao).

0378-7753/$ – see front matter © 2007 Published by Elsevier B.V.
doi:10.1016/j.jpowsour.2007.06.257

of the diffusion layer may result in blockage of pores, which in turn hinders the diffusion of methanol solution to the catalyst layer. This can lead to starvation of the reaction sites, and consequently, results in severe cell performance loss. Hence, investigation on the dynamic behavior of CO_2 gas bubbles in the anode channels will serve as a guide for the improvement on the performance of DMFC.

Flow visualization is an effective method to investigate either quantitatively or qualitatively the dynamic behavior of CO_2 gas bubbles in anode channels of an operating DMFC. Although the number of papers on DMFC has been published in a speed of over 100 papers per year since 2001, few research works have been reported in visualization experiments due to the difficulty in implementing it. Argyropoulos et al. [21] investigated visually CO_2 gas evolution process inside an operating DMFC, and the effects of operating parameters including different gas diffusion layer supporting materials, flow bed designs, cell sizes, exhaust manifold configurations as well as current density on the system gas management were studied. Scott et al. [22] reported a flow visualization study on CO_2 gas evolution and flow behavior with flow beds based on stainless steel mesh. It was found that the structure and the size of the stainless steel mesh have significant influence on the performance of the DMFC. Yang et al. [23] reported a visual study of CO_2 bubbles behavior in a single serpentine channel of a transparent DMFC anode. His study revealed the influence of current densities, cell orientation, methanol solution flow rates, etc. [23], and CO_2 bubbles distribution for different serpentine channels and parallel channels at different current density [24]. Lu and Wang [14] developed a 5 cm^2 transparent DMFC to visualize CO_2 bubbles flow in the anode and investigate the effects of pore structure and wettability on two-phase flow dynamics. Bewer et al. [25] revealed a novel method to investigate two-phase flow in liquid feed DMFC. The method was based on the decomposition of hydrogen peroxide solution (H_2O_2) to oxygen and water in aqueous media at the presence of a catalyst for in situ production of bubbles. An appropriate H_2O_2 concentration was used to set the same order of magnitude of the gas evolution rate as in a real DMFC. The flow homogeneity as a function of gas evolution rate, flow field and manifold design was investigated. Wong et al. [26] presented images of the cyclic bubbles behavior and the critical length of gas slugs in different flow channels to explore the effect of channel size on the CO_2 bubbles behavior.

In the present study, a transparent DMFC was constructed to visualize the two-phase flow of aqueous methanol solution and CO_2 gas bubbles by using a high-speed video camera. The dynamic behavior of CO_2 gas bubbles including emergence, growth, coalescence, and removal in the parallel anode channels of the operating cell was recorded in situ, and polarization curves were obtained to provide a fundamental understanding of the relationship between the behavior of CO_2 gas bubbles and the cell performance. A series of parametric studies, including aqueous methanol solution flow rate, temperature, concentration, and cell pressure difference between the anode and the cathode was performed to evaluate the effects on CO_2 gas bubbles behavior in the anode channels as well as the cell performance.

2. Experimental setup

2.1. MEA fabrication and transparent cell sample

In the present study, three MEAs (MEA1, MEA2 and MEA3) with an active area of 3.0 cm × 3.0 cm were fabricated in-house by hot-pressing two catalyzed electrodes to a pretreated Nafion® membrane 117 at 135 °C and 7 MPa for 2 min. The pretreatment for Nafion® membrane 117 follows a standard procedure: (i) boiling membrane in 5 wt.% H_2O_2 solution of 80 °C for 1 h; (ii) rinsing with DI water of 80 °C for 1 h; (iii) boiling membrane in 0.5 mol l^{-1} H_2SO_4 solution of 80 °C for 1 h; and (iv) rinsing with DI water of 80 °C for 1 h [23]. Carbon cloth from E-TEK was used as the backing support layer with 10 wt.% PTFE wet-proofing treatment for both the anode and the cathode electrodes. A mixture solution containing XC-72 carbon black and PTFE was coated on the carbon cloth to form the microporous layer with a carbon loading of 2 mg cm^{-2} and PTFE loading of 2 mg cm^{-2}. For MEA1, the catalyst loading on the anode side was 3.71 mg cm^{-2} with 40 wt.% Pt–Ru alloy (1:1 a/o) on Vulcan XC-72, and the catalyst loading on the cathode side was 2.45 mg cm^{-2} with 40 wt.% Pt on Vulcan XC-72. The catalyst loadings on the anode side and the cathode side of MEA2 were 2.71 mg cm^{-2} and 2.22 mg cm^{-2}, and those of MEA3 were 3.01 mg cm^{-2} and 2.98 mg cm^{-2}, respectively. One milligram per square centimeter of Nafion® was applied onto the surface of every electrode.

The transparent DMFC used in the present study is shown in Fig. 1. A pair of a stainless steel plates covered by a Lucite plate in the anode for flow visualization was adopted to be the bipolar plates of the cell. Nine parallel rectangular channels with dimensions of 2.1 mm (*W*), 1.0 mm (*H*), 30 mm (*L*), and 1.5 mm (*W*) for the rib were machined on the stainless steel plates to distribute the aqueous methanol solution and oxidant. Both the inlet and outlet manifold of the cell, shown at the bottom right corner

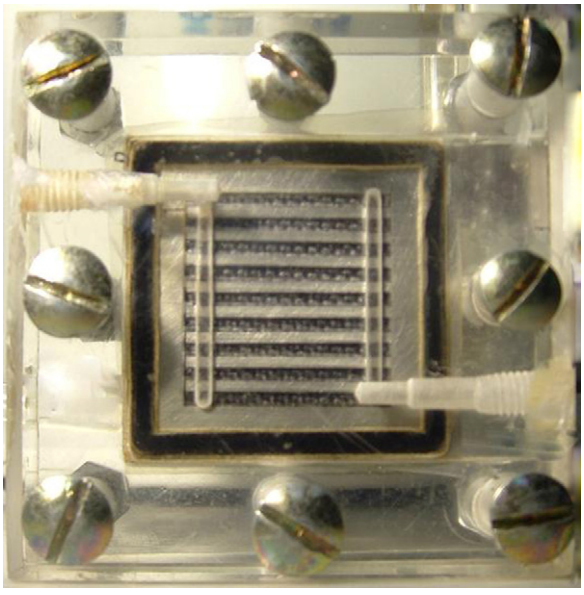

Fig. 1. Sample of the transparent DMFC.

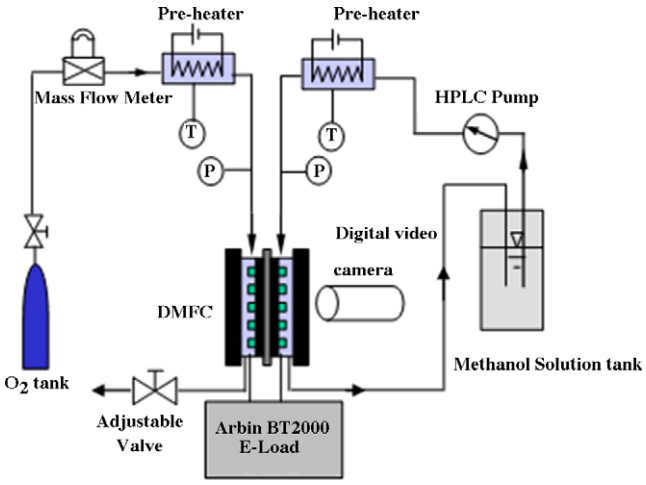

Fig. 2. Schematic experimental system of DMFC test.

and the top left corner in Fig. 1, respectively, were machined in the Lucite plates.

2.2. Experimental system and experimental conditions

The schematic experimental system for the performance of the transparent DMFC and the visualization of CO_2 bubbles in the anode channels is shown in Fig. 2. The experimental setup mainly consisted of an electronic-load system (Arbin BT2000), a HPLC micro-pump (Japan Servo Co. Ltd., KT42KM4-001), a mass flow meter (MKS M1008), two preheaters with temperature controller, and valves. The electronic-load system was used to control the operation conditions and to characterize polarization behaviors of the DMFC. The HPLC pump was employed on the anode side to deliver the methanol solution to the cell. The mass flow meter was employed to regulate the flow rate of dry oxygen (99.99% in purity) on the cathode side. The valves were applied to control the back pressure at the exits of the anode and the cathode. The preheaters with temperature controller were used to preheat both the methanol solution and the oxygen to a desired temperature prior to entering the cell. A digital camcorder (Sony DCR-PC110E) with 30 frames s^{-1} was used to record visualization results of the two-phase flow in the anode channels and still pictures were captured according to the time sequence when the movie was edited offline. Also, a camera Redlake MotionXtra HG-100K with 125 frames s^{-1} for the present study was utilized to obtain images of CO_2 bubbles in a single anode channel. A halogen spot lamp was used to illuminate the fuel cell in order to capture clear pictures of the bubbles flow in the channel.

Results presented in the following sections were obtained with a constant gas flow rate of 500 ml min^{-1}, a constant preheated temperature (60 °C) for oxygen, and atmospheric pressure (0.1 MPa) for the aqueous methanol solution. Other experimental conditions for the parameters studies are listed in Table 1.

3. Results and discussion

3.1. Dynamic behavior of CO_2 gas bubbles in a straight anode channel of DMFC

A set of time evolution images is shown in Fig. 3 to show the dynamic behavior of CO_2 gas bubbles in a straight anode channel of the cell. As can be seen from the figure, CO_2 gas bubbles first emerged around the corner between the channel rib and the surface of the porous diffusion layer (t = 1 s, 2 s), and adhered to the surface of the diffusion layer forced by surface tension. As time progressed (t = 3–7 s), CO_2 gas bubbles successively emerged at other different sites of the porous diffusion layer surface, meanwhile the previous bubbles around the corner grew bigger, hence numerous CO_2 gas bubbles were observed. It can be explained that the tight assemblage of the cell breaks the carbon cloth fibres near the channel ribs to provide the favorable sites for the emergence of CO_2 gas bubbles. It was also noted that the larger pores at the intersection of the carbon cloth fibre bunches were favorable sites for the emergence of CO_2 gas bubbles from the porous diffusion layer due to the lower flow resistance for larger porosity. Following the growth, CO_2 gas bubbles began to coalesce into bigger bubbles and expanded from the corner of the rib toward the center of the channel, which resulted in increasing area coverage on the porous diffusion layer surface. Once the size of the coalesced CO_2 gas bubbles reached the width of the channel, the bubbles elongated along the channel and formed the discontinuous gas slugs, which then blocked the crosscurrent flow of the aqueous methanol solution (t = 12 s, 13 s). At 14 s shown in Fig. 3, a large CO_2 gas slug was formed from coalescence of discontinuous gas slugs and covered the entire porous diffusion layer surface. Eventually, the large CO_2 gas slug was pushed out of the channel by the crosscurrent flow of the aqueous methanol solution. This was accompanied by the sweeping of all pre-existing smaller bubbles downstream and cleaning the channel (t = 16 s). The periodic scenario of CO_2 gas bubbles movement and the

Table 1
Experimental conditions

Items	Flow rate of methanol solution (ml min^{-1})	Temperature of methanol solution (°C)	Concentration of methanol solution (mol l^{-1})	Cathode pressure (MPa)	MEA
Bubble dynamics	10	60	2	0.136	MEA2
Effect of flow rate	Variable	60	2	0.136	MEA1
Effect of temperature	10	Variable	2	0.136	MEA1
Effect of concentration	10	60	Variable	0.136	MEA1
Effect of pressure difference	10	60	2	Variable	MEA3

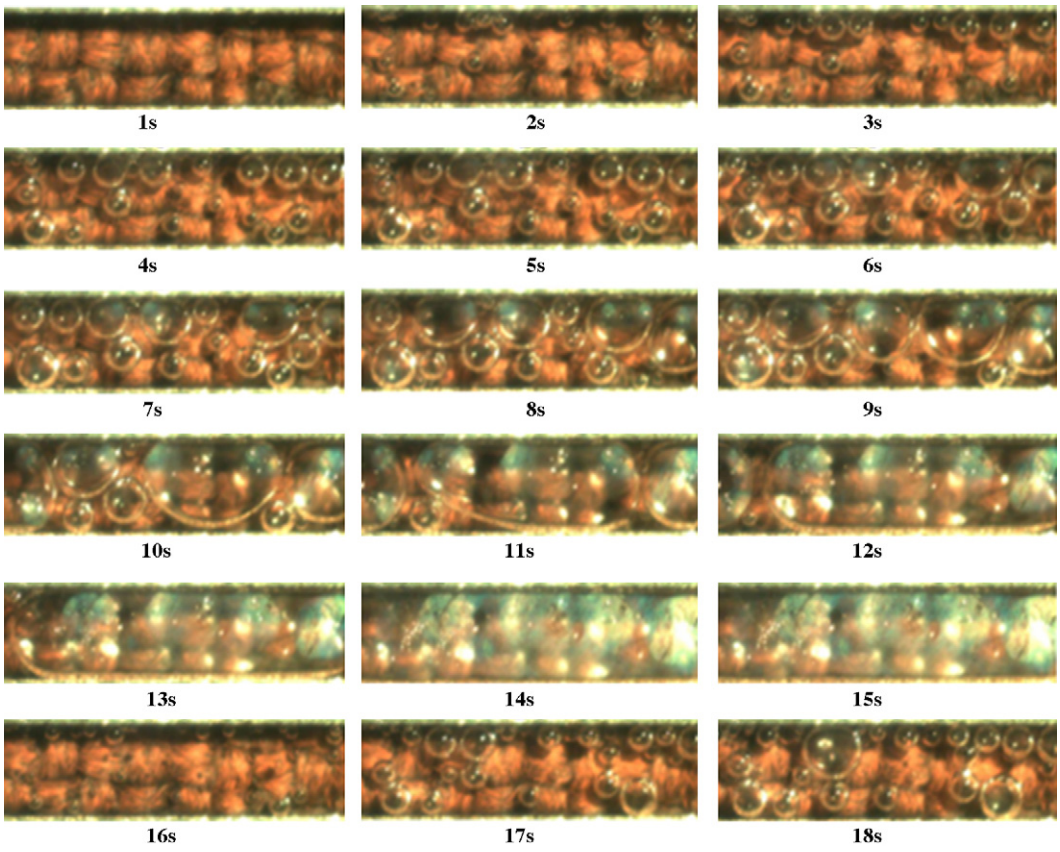

Fig. 3. Time evolution images of CO_2 gas bubbles in a parallel anode channel.

two-phase flow pattern, including emergence, growth, coalescence, gas slug, and removal, repeated again from $t = 16$ s on. This can be understood by considering the balance of the forces exerted on the CO_2 gas bubbles. The shear stress and the pressure difference resulted from the aqueous methanol solution flowing around CO_2 gas bubbles, the surface tension which is related to the properties of the bubble and the rib as well as the porous diffusion layer surface, and the coalescence of gas bubbles synthetically determine the dynamic behavior of CO_2 gas bubbles in the channel. A discrete distribution of CO_2 gas bubbles early emerged in the channel is dominated by the surface tension, and then the shear stress and the static pressure difference take over the surface tension to succeed in the removal of the coalesced gas slugs that block the channel.

3.2. *Effect of aqueous methanol solution flow rate*

Fig. 4 shows the distribution of CO_2 gas bubbles in the parallel anode channels at aqueous methanol solution flow rates of 2 ml min^{-1}, 4 ml min^{-1}, 8 ml min^{-1}, and 10 ml min^{-1}, respectively, for the same current density of 45 mA cm^{-2}. It can be seen that as the aqueous methanol solution flow rate increased, the individual CO_2 gas bubbles emerging into the channels became smaller, and the coalescent gas slugs became shorter and less as well. When the aqueous methanol solution flow rate reached 10 ml min^{-1}, the coalescence of the gas bubbles was not observed and CO_2 gas bubbles distributed discretely in the channels and moved out from the channels in discrete bubbles. This can be explained by that higher flow velocity caused higher shear stress and static pressure difference on the interface of CO_2 gas bubbles. This makes it difficult for the smaller bubbles to coalesce. Breaking up the gas slugs in the channels facilitates the methanol solution to the catalyst sites on the catalyst layer surface through the porous diffusion layer and improves the cell performance.

The effect of the aqueous methanol solution flow rate on the cell performance is shown in Fig. 5. For the case tested, the open circuit voltage and the cell performance at low current density were similar for different aqueous methanol solution flow rates. When the aqueous methanol solution flow rate increased from 2 ml min^{-1} to 8 ml min^{-1}, the cell performance improved at higher current densities. However, when the aqueous methanol solution flow rate increased over 8 ml min^{-1}, say 10 ml min^{-1}, the cell performance did not show further improvement. This can be explained by the effect of the aqueous methanol solution flow rate on the dynamic behavior of CO_2 gas bubbles. As was discussed previously, higher aqueous methanol solution flow rate accelerates the removal of CO_2 gas bubbles in the channels, resulting in the enlarged effective contact area between the aqueous methanol solution and the porous diffusion layer. It enhances the mass transfer of methanol to the catalyst sites, hence improved the cell performance. However, when the aqueous methanol solution flow rate is excessive, less CO_2 gas bubbles remain in the channels, and sufficient methanol solution

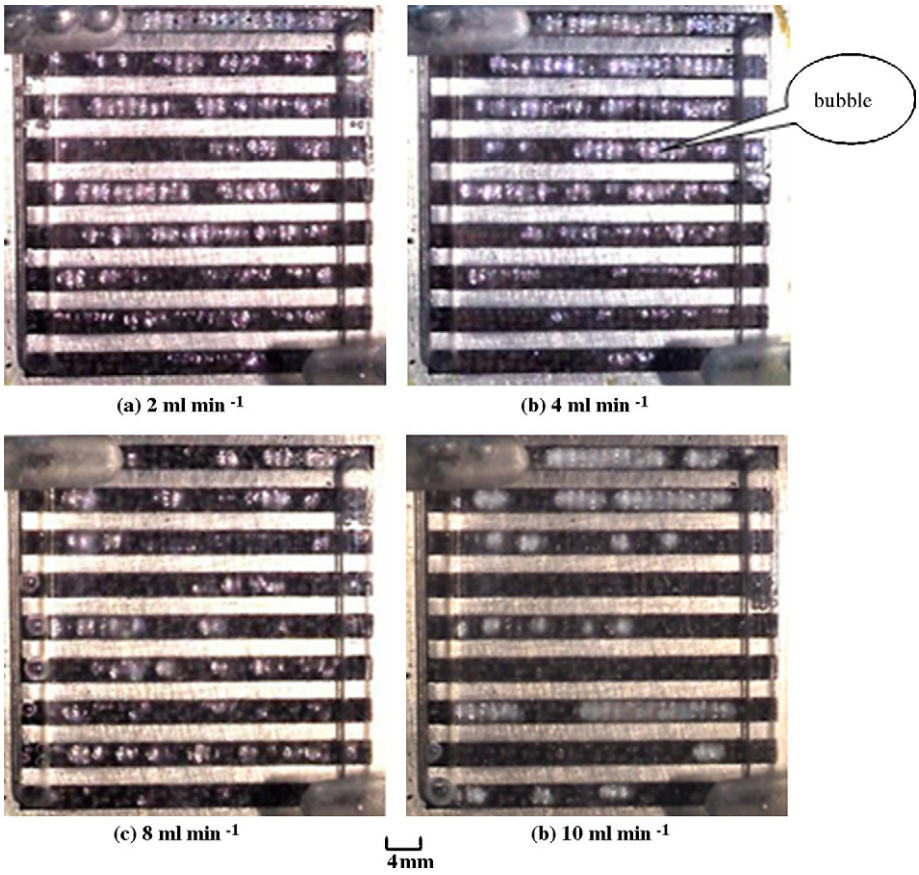

Fig. 4. Distribution of CO_2 gas bubbles in anode channels at different aqueous methanol solution flow rate.

can reach the catalyst sites. Therefore the dominative process for the cell performance is no longer mass transfer of methanol but the electrochemical reaction on the catalyst layer surface. Meanwhile, high aqueous methanol solution flow rate will result in high static pressure in the anode channel, i.e. high pressure difference between the anode and cathode of the cell. This will increase the methanol crossover from the anode to the cathode, which negates the benefit from the increased mass transfer of the methanol on the anode side. This does not lead to further cell performance improvement. It can be predicted that the cell performance may deteriorate if the aqueous methanol solution flow rate increases excessively.

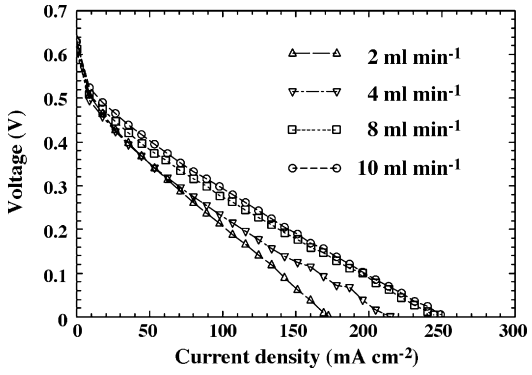

Fig. 5. The effect of the aqueous methanol solution flow rate on the cell performance.

3.3. Effect of aqueous methanol solution temperature

Images of CO_2 gas bubbles in the parallel anode channels for different aqueous methanol solution feed temperature at 30 °C, 40 °C, and 60 °C, respectively, for the same current density of 50 mA cm^{-2} are shown in Fig. 6. During the experiments, it was observed that the dynamic behavior of CO_2 gas bubbles including emergence, growth, coalescence, and formation of the gas slugs was similar at different methanol solution feed temperature. The quantity of CO_2 gas bubbles and large gas slugs increased in the channels at higher aqueous methanol solution feed temperature, cf. 60 °C. It took more coverage area of the porous diffusion layer and hindered the access of methanol to the catalyst sites, hence resulting in deterioration of the cell performance. This phenomenon results from the increasing specific volume as well as decreasing solubility of carbon dioxide gas in the aqueous methanol solution due to increasing temperature at a fixed pressure.

The effect of the aqueous methanol solution feed temperature on cell performance is presented in Fig. 7. One can see that the cell performance improved and the duration time for discharge increased with increasing aqueous methanol solution feed temperature. The main reasons should be attributed

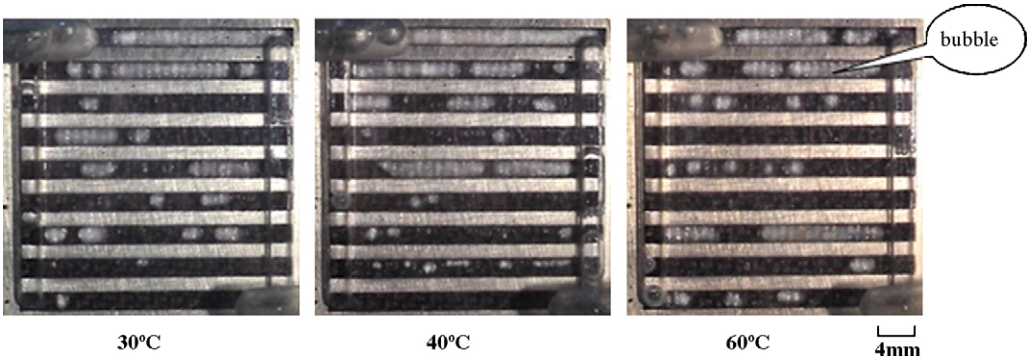

Fig. 6. Distribution of CO_2 gas bubbles in the anode channels for different aqueous methanol solution feed temperatures.

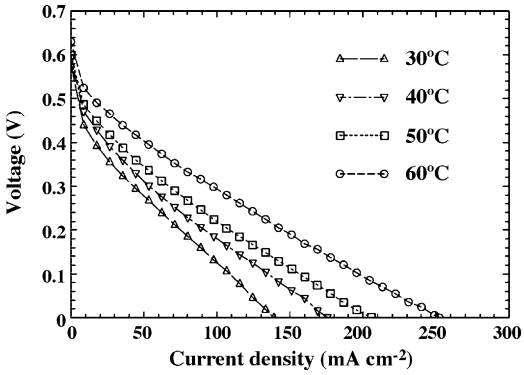

Fig. 7. The effect of the aqueous methanol solution feed temperature on the cell performance.

to the enhanced activity of the catalyst with increasing temperature, which accelerates the electrochemical reaction in the cell. Besides, an increase in temperature will enhance the thermal movement of the methanol molecules and then increase the diffusion coefficient of the methanol solution. As a result, the mass transport of methanol to the catalyst sites as well as the products of the electrochemical reaction to the channels is improved. This reduces the concentration polarization of the operating cell. It is clear that the effect of the enhanced activity of the catalyst and increasing diffusion coefficient of methanol surmounts that of numerous CO_2 gas bubbles and large gas slugs, thus leading to the improvement of the cell performance.

3.4. Effect of pressure difference between anode and cathode

Fig. 8 shows the distribution of CO_2 gas bubbles in the parallel anode channels at different pressure difference between the anode and the cathode of the cell. The pressure difference varied from 0 MPa to 0.136 MPa by adjusting the operation pressure of oxygen in the cathode while the operation pressure of the aqueous methanol solution in the anode was kept constant. As can be seen from the images, the quantity of discrete CO_2 gas bubbles and large gas slugs formed by coalescence increased with increasing pressure difference between the anode and the cathode. It can be analyzed that the motion of CO_2 gas bubbles in the anode is driven primarily by the concentration gradient accompanied with the pressure gradient between the catalyst layer and the channels. Increasing the pressure difference between the anode and the cathode induces an enhancement on convective flow, which enhances the transport of CO_2 gas bubbles from the catalyst layer through the porous diffusion layer to the channels. As a result, the removal of CO_2 gas bubbles from the porous diffusion layer leaves more pores for methanol diffusing to the catalyst sites. On the other hand, the increasing quantity of CO_2 gas bubbles and gas slugs in the channels takes a large coverage area on the porous diffusion layer surface and blocks the channels if there is lower flow rate of the aqueous methanol solution.

Fig. 9 shows the polarization curves at different pressure difference between the anode and the cathode. There was a

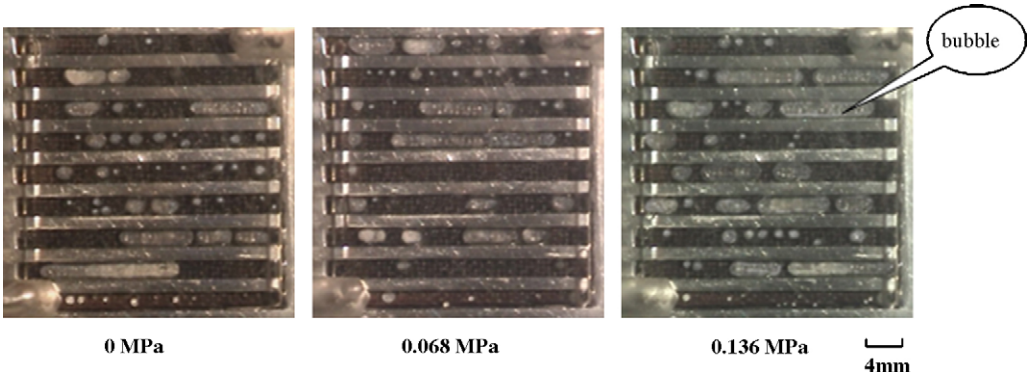

Fig. 8. Distribution of CO_2 gas bubbles in the anode channels at different pressure differences between the anode and the cathode.

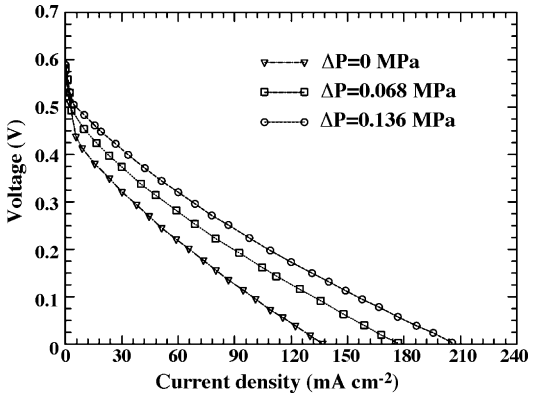

Fig. 9. Effect of the pressure difference between the anode and the cathode on the cell performance.

definite improvement on the cell performance with increasing pressure difference from 0 MPa to 0.136 MPa. The main reasons contributing to the improvement lie on the following two aspects. One is that higher operation oxygen pressure leads to higher density and solubility of oxygen in Nafion in the cathode, hence induces higher oxygen concentration on the catalyst sites. Because the deoxidization velocity in the cathode is nearly proportional to the oxygen concentration on the catalyst sites (Pt), the higher oxygen concentration in the cathode will definitely accelerate the electrochemical reaction velocity. Another is that an increase in the operation pressure in the cathode weakens the methanol crossover, which depresses the poisoning of the catalyst in the cathode. Comprehensively taking account of the blockage in the anode channels by increasing CO_2 gas bubbles and larger gas slugs, improved diffusion of methanol in the porous diffusion layer as well as higher oxygen concentration in the cathode, and less methanol crossover, the cell performance improves with increasing pressure difference between the anode and the cathode. However, higher pressure raises the difficulty for sealing the cell.

3.5. Effect of methanol concentration

Fig. 10 presents the effect of methanol concentration on the cell performance at 0.5 mol l^{-1}, 1 mol l^{-1}, and 2 mol l^{-1}, respectively. It is noted that the cell performance changed diversely with increasing methanol concentration at different current densities. For high methanol concentration, the open circuit voltage and the output voltage decreased when the cell was operating at low current density. This can be explained by the fact that diffusion dominates the methanol crossover in the cell. When the cell works at low current densities, an increase in the methanol feed concentration induces redundant methanol on the catalyst sites, which exceeds the actual need for the electrochemical reaction in the anode. Redundant methanol remaining in the anode increases the methanol concentration to lead to the augmentation of methanol crossover, hence deteriorating the cell performance. However, the limiting current of the cell increases with increasing methanol concentration when the cell worked at higher current densities. The cell performance improved significantly by increasing the methanol concentration from 0.5 mol l^{-1} to 1 mol l^{-1} compared to the increase from 1 mol l^{-1} to 2 mol l^{-1}. This can be attributed to increasing methanol concentration, which satisfies the additional requirement of the electrochemical reaction in the anode due to higher current densities. The cell performance reached the best when the methanol concentration was 2 mol l^{-1} in the present study. But then, it should be mentioned that the methanol crossover might be aggravated if the methanol concentration is excessive. If that happens, the mixed potential and the poisoning of the catalyst will be induced in the cathode, which results in the cell performance loss. Therefore, it can be predicted that the cell performance will be deteriorated if the methanol feed concentration is increased further [27].

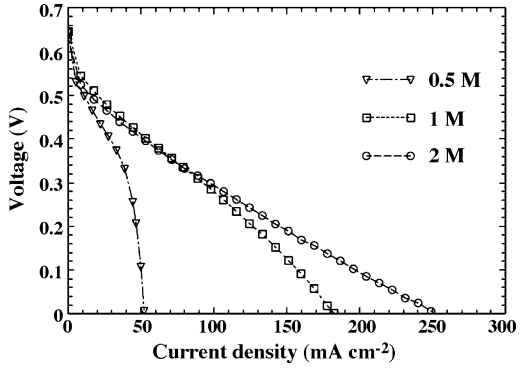

Fig. 10. Effect of the methanol concentration on the cell performance.

4. Conclusions

In the present study, a transparent DMFC with an active area of 9 cm^2 was developed to visualize CO_2 gas bubbles flow in the anode channels. Parametric studies of the aqueous methanol solution flow rate, temperature, concentration, and the pressure difference between the anode and the cathode of the cell were carried out to assess the effects on CO_2 gas bubbles behavior in the anode channels and the cell performance. It was observed that CO_2 gas bubbles first emerged around the corner of the porous diffusion layer and the channel ribs and formed large gas slugs by growth and coalescence in the channel. The pores around the corner and on the intersection of the carbon cloth fibres were favorable sites for the emergence of CO_2 gas bubbles. Increasing the flow rate of the methanol solution accelerated the removal of the discrete CO_2 gas bubbles which enhanced the mass transfer of the methanol, hence improving the cell performance. While the performance cannot be improved further by increasing the flow rate over a particular value. Increasing the feed temperature of the methanol solution reduced the solubility of CO_2 gas in the aqueous methanol solution, hence increasing the quantity of CO_2 gas bubbles in the channels. The cell performance improved at high feed temperature owing to the enhancement of diffusion of methanol and acceleration of the catalysis. High methanol concentration resulted in high cell performance. The excessive methanol concentration will aggravate the methanol crossover to lead to the cell performance loss. More CO_2 bubbles and larger gas slugs appeared in the channels with increasing pressure difference between the anode and the cathode, but the cell performance improved with high oxygen concentration on

the catalyst surface and less methanol crossover due to high operating pressure in the cathode.

Acknowledgements

The authors are grateful for the support of the National Natural Science Foundation of China (No. 90410005), the Excellent Young Teachers Program of MOE, PR China ([2003]355#).

References

[1] C.K. Dyer, J. Power Sources 106 (2002) 31–34.
[2] K. Cowey, K.J. Green, G.O. Mepsted, R. Reeve, Curr. Opin. Solid State Mater. Sci. 8 (2004) 367–371.
[3] P. Argyropoulos, K. Scott, A.K. Shukla, C. Jackson, J. Power Sources 123 (2003) 190–199.
[4] Z.B. Wang, G.P. Yin, P.F. Shi, J. Power Sources 163 (2007) 688–694.
[5] W.P. Liu, C.Y. Wang, J. Electrochem. Soc. 154 (2007) B352–B361.
[6] J.K. Lee, J. Choi, S.J. Kang, J.M. Lee, Y. Tak, J. Lee, Electrochim. Acta 52 (2007) 2272–2276.
[7] S.K. Kamarudin, W.R.W. Daud, S.L. Ho, U.A. Hasran, J. Power Sources 163 (2007) 743–754.
[8] K. Fei, C.W. Hong, Microfluid. Nanofluid. 3 (2007) 77–88.
[9] V.A. Danilov, J. Lim, I. Moon, H. Chang, J. Power Sources 162 (2006) 992–1002.
[10] D. Chakraborty, I. Chorkendoff, T. Johannessen, J. Power Sources 162 (2006) 1010–1022.
[11] S. Rajasekaran, R. Ammar, K. Reifsnider, L. Achenie, A. Mohamed, G. Zhang, M.J. Ahmed, Fuel Cell Sci. Technol. 2 (2005) 141–144.
[12] G.B. Jung, A. Su, C.H. Tu, F.B. Weng, J. Fuel Cell Sci. Technol. 2 (2005) 81–85.
[13] M. Sudoh, T. Hakamata, K. Furukawa, K. Okajima, Int. J. Green Energy 1 (2004) 153–165.
[14] G.Q. Lu, C.Y. Wang, J. Power Sources 134 (2004) 33–40.
[15] M. Kunimatsu, T. Okada, Electrochem. Solid-State Lett. 7 (2002) A389–A390.
[16] M.G. Izenson, R.W. Hill, J. Fuel Cell Sci. Technol. 1 (2004) 10–17.
[17] H. Yang, T.S. Zhao, Q. Te, J. Power Sources 142 (2005) 117–124.
[18] H. Yang, T.S. Zhao, Q. Ye, Electrochem. Commun. 6 (2004) 1098–1103.
[19] Q. Ye, T.S. Zhao, J. Prabhuram, Electrochem. Solid-State Lett. 8 (2005) A52–A54.
[20] C.W. Wong, T.S. Zhao, Q. Ye, J.G. Liu, J. Power Sources 155 (2006) 291–296.
[21] P. Argyropoulos, K. Scott, W.M. Taama, J. Appl. Electrochem. 29 (1999) 661–669.
[22] K. Scott, P. Argyropoulos, P. Yiannopoulos, W.M. Taama, J. Appl. Electrochem. 31 (2001) 823–832.
[23] H. Yang, T.S. Zhao, Q. Ye, J. Power Sources 139 (2005) 79–90.
[24] H. Yang, T.S. Zhao, Electrochim. Acta 50 (2005) 3243–3252.
[25] T. Bewer, T. Beckmann, H. Dohle, J. Mergel, D. Stolten, J. Power Sources 125 (2004) 1–9.
[26] C.W. Wong, T.S. Zhao, Q. Ye, J.G. Liu, J. Electrochem. Soc. 152 (2005) A1600–A1605.
[27] Y.D. Ding, Q. Liao, X. Zhu, L.J. Bao, J. Power Eng. 26 (2006) 599–603.